Nuclear Instruments and Methods in Physics Research A ▮ (▮▮▮▮) ▮▮▮–▮▮▮

Contents lists available at ScienceDirect

Nuclear Instruments and Methods in Physics Research A

journal homepage: www.elsevier.com/locate/nima

A new multianodic large area photomultiplier to be used in underwater neutrino detectors

S. Aiello [a], A. Amore [b], M. Anghinolfi [c], M. Battaglieri [c], A. Bersani [d,c], M. Brunoldi [d], L. Caponetto [a], R. De Vita [c], K. Fratini [c], A. Grimaldi [a], V. Kulikovskiy [e], E. Leonora [a], D. Lo Presti [b,a], G. Mini [d], S. Minutoli [c], P. Musico [c], M. Osipenko [c], G. Ottonello [c], D. Piombo [c], N. Randazzo [a], G. Ricco [d,c], M. Ripani [c], A. Rottura [c], G.V. Russo [b,a], A. Savasta [b], D. Sciliberto [a], E. Shirokov [e], V. Sipala [b,a], M. Taiuti [d,c,*], S. Urso [a], S. Zavatarelli [c,1]

[a] INFN Sezione Catania, Via S. Sofia 64, 95123 Catania, Italy
[b] Dipartimento di Fisica e Astronomia, Università di Catania, Via S. Sofia 64, 95123 Catania, Italy
[c] INFN, sezione di Genova, Via Dodecaneso 33, I-16146 Genova, Italy
[d] Dipartimento di Fisica dell'Università di Genova, Via Dodecaneso 33, 16146 Genova, Italy
[e] Institute of Nuclear Physics, Moscow State University, 119899 Moscow, Russia

ARTICLE INFO

Article history:
Received 22 August 2008
Received in revised form
18 February 2009
Accepted 30 March 2009

Keywords:
Photomultiplier
Neutrino astronomy
Deep sea detector

ABSTRACT

In this article we describe the properties of a new 10-in. hemispherical photomultiplier manufactured by Hamamatsu. The prototype has a segmented photocathode and four independent amplification stages. The photomultiplier is one of the main components of a newly designed direction-sensitive optical module to be employed in large-scale underwater neutrino telescopes. The R&D activity has been co-funded by the INFN and the KM3NeT Consortium. The prototype performance fully meets with the design specifications.

1. Introduction

One important component of an underwater neutrino telescope is the photodetector required to collect the Cherenkov light produced by the ionizing particles that originate from the interaction of the neutrino [1–4]. To efficiently cover 1 km^3 detection volume it would be necessary to deploy $\approx 10^4$ photomultipliers whose main requirements are a relatively large photocathode area, high gain, low noise, low after pulse rate and good timing resolution for single photon detection, the exact values depending on the detector design. The current minimum requirements for such detectors, taken from the KM3NeT Conceptual Design Report [5], are reported in Table 1.

The aim of the European KM3NeT [6] Consortium is to define the Technical Design Report of the km^3 detector to be deployed in the Mediterranean Sea. Several new ideas are being developed to improve the performance of the optical modules, e.g. the prototyping activity in progress at CERN [7], aimed at applying the ideas that originated the Philips "SMART" XP2600 [8] and the later QUASAR-370 [9] to the production of a large area, high single photon resolution detector; or the work being carried on at NIKHEF with the idea of segmenting the photocathode area in order to count the number of photons, by replacing a single 10-in. PMT with at least 12 3-in. PMTs [10].

Monte Carlo simulations show that if it were possible to identify the Cherenkov light direction, reconstruction efficiency would improve in particular for short tracks related to low energy (below 10 TeV) neutrinos or to tracks that partially cross the detector. As an example, in Fig. 1 we report the effect of the information on the direction of the detected Cherenkov light on the response of a km^3 detector à la NEMO [12,13].

In the KM3NeT research framework we have proposed the implementation of this feature by means of a multianodic 10-in. photomultiplier coupled to a light guide system so that all the Cherenkov light arriving from the same direction is focused on a well-defined sector of the photocathode. The basic working principles have been discussed in Ref. [14]. The conceptual design is based on a multi-anodic position sensitive

* Corresponding author at: Dipartimento di Fisica dell'Università di Genova, Via Dodecaneso 33, 16146 Genova, Italy. Tel.: +39 010 3536203; fax: +39 010 313358.
E-mail address: Mauro.Taiuti@ge.infn.it (M. Taiuti).
[1] In cooperation with the KM3NeT Consortium.

0168-9002/$ - see front matter © 2009 Elsevier B.V. All rights reserved.
doi:10.1016/j.nima.2009.03.235

Table 1
KM3NeT technologies detector requirements.

Time resolution (for a single photon, photomultiplier + electronics)	<2 ns
Position resolution	<40 cm
Charge dynamic range	$\approx 100/25$ ns
Two-hit time separation	<25 ns
Coincidence acceptance	$>50\%$
False coincidences	Dominated by random coincidences from marine background photons
Dark noise rate	$<20\%$ of the ^{40}K rate
Failure rate of the optical modules	$<10\%$ over 10 years without major maintenance

The table is taken from Ref. [5].

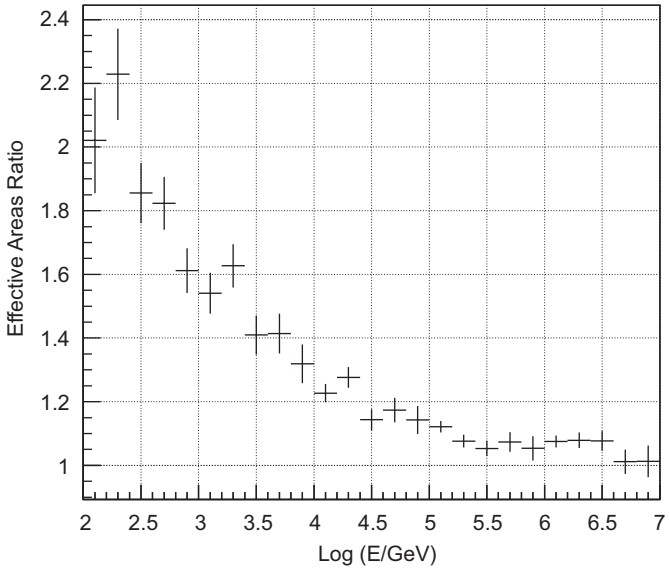

Fig. 1. The ratio of the effective areas of the NEMO detector equipped with direction-sensitive optical modules and the standard NEMO detector.

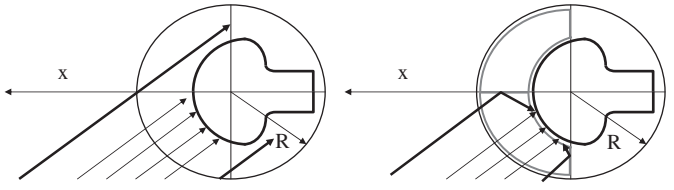

Fig. 2. Left: behaviour of the classical optical module: all the Cherenkov light coming from a specific direction illuminates the whole photocathode surface. Right: the mirrors concentrate the light coming from a specific direction onto a single sector of the photocathode surface.

10-in. photomultiplier coupled to a set of mirrors. The mirrors are realized with 3M Radiant Mirror Films glued onto 2 mm Plexiglas foils. The 3M films are multi-layer polymeric films with a reflectivity larger than 95% in the wavelength interval 400–700 nm [15]. Fig. 2 shows how the side view of the optical module changes with the mirrors: all photons arriving from the same direction are focused by the mirror system onto a single sector of the multi-anodic photomultiplier. In this way the angular acceptance of the optical module is divided into four with only a small overlap along the symmetry axis of the photomultiplier. The result is greater accuracy in the evaluation of the direction of the detected light is increased.

Large area multianodic photomultipliers are not commercially available and, therefore, we contacted the leading companies in the field in order to investigate the feasibility of producing such a device. In this paper we present the performances of the two prototypes of a 10-in. 4-anodic photomultiplier manufactured by Hamamatsu. The two samples (ZF0021 and ZF0025) are of the same shape as the 10-in. Hamamatsu R7081. Like the Hamamatsu R7081, the amplification chain includes 10 dynode stages. The photomultiplier hosts four separate dynode chains with common voltages. To perform the tests the photomultiplier was connected to a resistive voltage divider produced according to the specifications provided by Hamamatsu.

2. Testing facility

The testing facility used to measure the characteristics of the large area photomultipliers is based on a light-tight dark box, with dimensions $2.0 \times 1.7 \times 1.5\,\mathrm{m}^3$, equipped with a frame designed to host the photomultiplier, a moving system required to scan the photocathode surface with the light source and a PMT used as a monitor to check the stability of the light source. The light source, located outside, is a 410 nm PICOQUANT pulsed laser [16], with a pulse width of 60 ps, whole frequency can vary in the range of 0–40 MHz using an external generator. For a precise calibration of the source in single photoelectron condition, we used a DEP Hybrid PhotoDiode PP0270K. The laser optical power range was calibrated using tan OPHIR PD-300 bolometer [17], to measure the linearity of the phototube.

The light pulses are brought into the dark box by a 50 μm multimode optical fibre, and then split into two fibres to illuminate the PMT under test and the reference PMT. In order to study the characteristics of the photomultiplier's response locally, the fibre is mounted on a moving system that allows the entire photocathode area to be scanned with a 5 mm diameter single-photon pulsed beam. The moving system is constituted by a semicircular guide capable of rotating vertically in the angular interval 0–180° and a frame holding the optical fibre that can move from one extremity of the guide to the

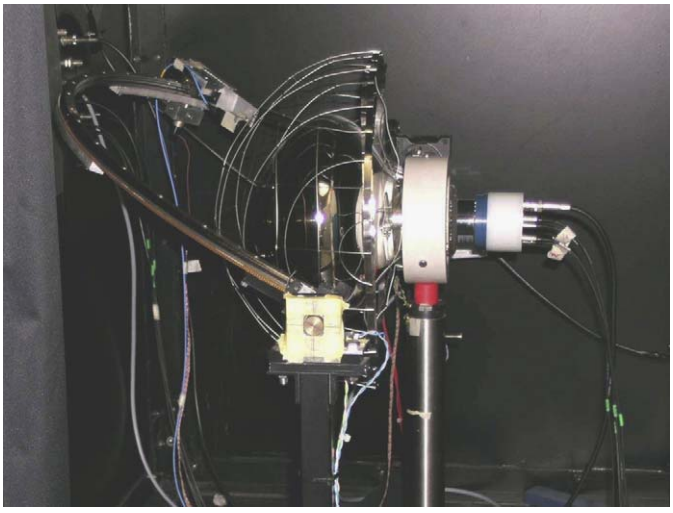

Fig. 3. The picture of the interior of the dark box with the moving system and the photomultiplier with the mu-metal cage.

Please cite this article as: S. Aiello, et al., Nucl. Instr. and Meth. A (2009), doi:10.1016/j.nima.2009.03.235

other. The movement of the two elements, obtained with two independent motors controlled by a PC, allows the whole hemispherical photocathode surface to be scanned with the extremity of the optical fibre continually pointing toward the centre of the semicircular guide. A picture of the interior of the dark box is shown in Fig. 3.

A custom software developed in LabView controls the sequence of all the operations, in particular the source movement and the data acquisition. On the basis of the geometric characteristics of the PMT, the software calculates the distribution of the measured points on the photocathode surface, making it possible to choose the number of points and the angular step of the scan.

A more detailed description of the testing facility and of the measurements reported in this paper can be found in Refs. [18,19].

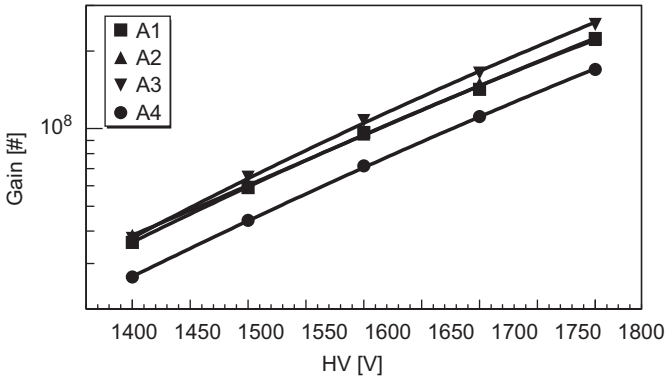

Fig. 4. The gain for each anode of the ZF0021 as a function of the applied HV. The behaviour of A1 and A2 is almost the same and the points overlap.

Table 2
Summary of the ZF0021 photomultiplier gain properties according to the power law $G = G_0 + G_1 * (HV[V]/1400)^m$.

Anode	A1	A2	A3	A4
G_0 [$\times 10^7$]	0.04	0.85	0.00	0.19
G_1 [$\times 10^7$]	3.5	3.0	3.8	2.5
m	7.23	7.83	7.66	7.63

3. Prototype performances

3.1. PMT gain

The gain of the photomultiplier was measured by studying the change in position of the single-photon peak for each anode as a function of the HV value using a calibrated charge ADC. The result for the ZF0021 sample is presented in Fig. 4: the experimental points have been fitted using the power law $G = G_0 + G_1 * (HV[V]/1400)^m$. Three anodes (A1, A2 and A3 according to the Hamamatsu numbering) behave similarly; the fourth anode A4 has a smaller gain ($\approx -25\%$ at 1500 V). The dependence on the HV value is approximately the same. The parameters of the fit for sample ZF0021 are given in Table 2. Similar behaviour was observed with the ZF0025 where the A4 anode shows a gain $\approx$ 20% smaller. According to Hamamatsu this common behaviour is accidental and is related to the quality of the dynodes [20].

The typical single photon pulse shape distribution is reported in Fig. 5.

3.2. Overall response

In this section we report the response of the photomultiplier when the whole photocathode surface was uniformly illuminated with a plane-wave pulsed beam. The applied voltage was 1550 V corresponding to a nominal gain of $\approx 5 \times 10^7$. All measurements were performed at room temperature. To entirely illuminate the photocathode with a plane-wave pulsed beam the photomultiplier was positioned away from the light source, at a calibrated distance of 0.70 m.

The linearity was measured for each anode separately. Each anode shows rather good linearity up to 100 photoelectrons as shown in Fig. 6 for anode A1 in the ZF0025 sample.

In Fig. 7 the pulse height is shown for each anode in the ZF0025 sample when illuminated with a flux such that the

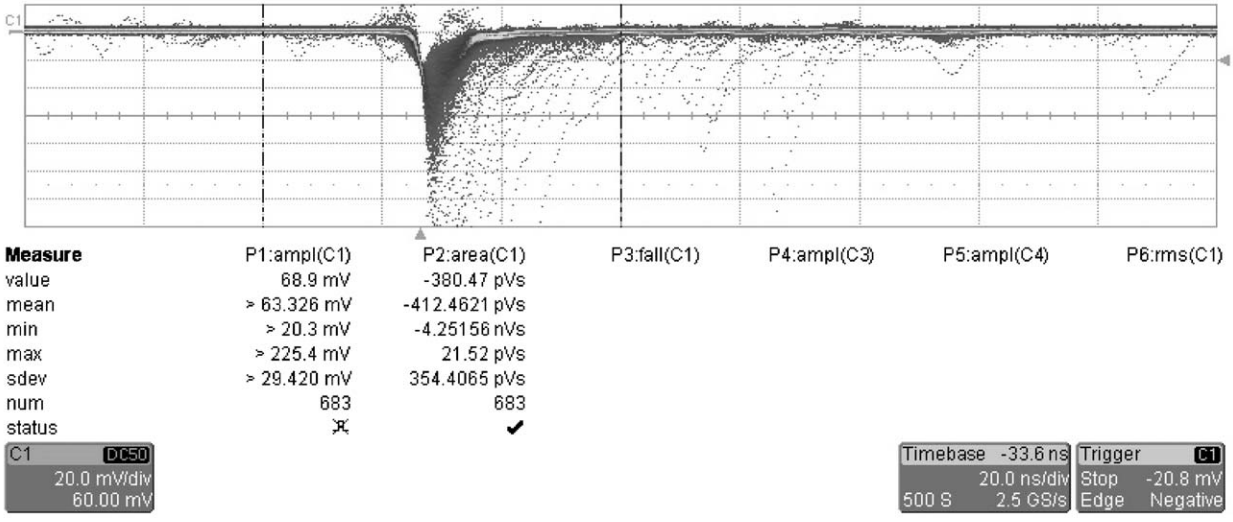

Fig. 5. Typical single photon pulse shape distribution. Each division on the x axis corresponds to 20 ns.

Please cite this article as: S. Aiello, et al., Nucl. Instr. and Meth. A (2009), doi:10.1016/j.nima.2009.03.235

contamination to the single photoelectron peak from events with 2 or more photoelectrons is smaller than 1%. The peak to valley ratio ranges between 2.7 and 3.1 and the single photoelectron peak shows a width (σ_E/E) between 30.6% and 37.5%. These values are generally comparable to those of the R7081-20, XP1804/D2 and R8055 photomultipliers studied by the ANTARES Collaboration team [21].

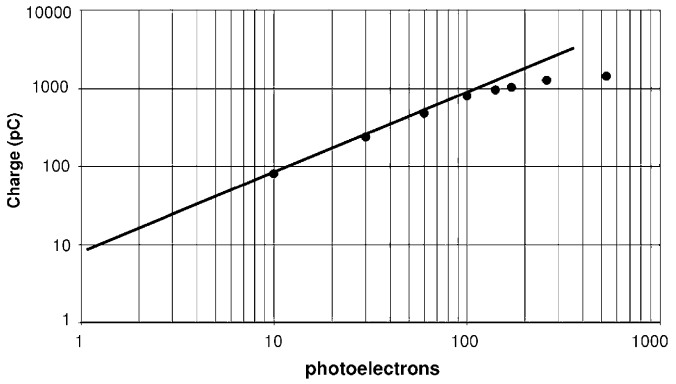

Fig. 6. The linearity response of anode A1 in the ZF0025 sample.

In Fig. 8 the timing response is shown for each anode. The measurement was performed setting the discriminator threshold to 20 mV corresponding to about 1/3 of the single photoelectron peak as determined from the pulse height measurement. The Transit Time Spread (TTS), defined as the FWHM of the distribution, ranges between 3.5 and 4.6 ns, exceeding the corresponding values of the Hamamatsu R7081-20 [21] but within the KM3NeT specifications [23].

In Table 3 a summary of the previous measurements is reported. Excluding the smaller gain of anode A4, the performances of the four anodes are comparable.

With the same threshold the dark current pulses of each anode are of the order of 1 kHz. This value is equal to that measured with the same setup on standard R7081 Hamamatsu tubes.

The last measured quantity is the fraction of spurious pulses following the procedures given in Ref. [11]. The definition of the measured quantities is graphically represented in Fig. 9. We identified four different types of secondary pulse according to the following definitions:

- Pre-pulse: pulses arriving at 10–80 ns before the main pulse, when the main pulse is not present.

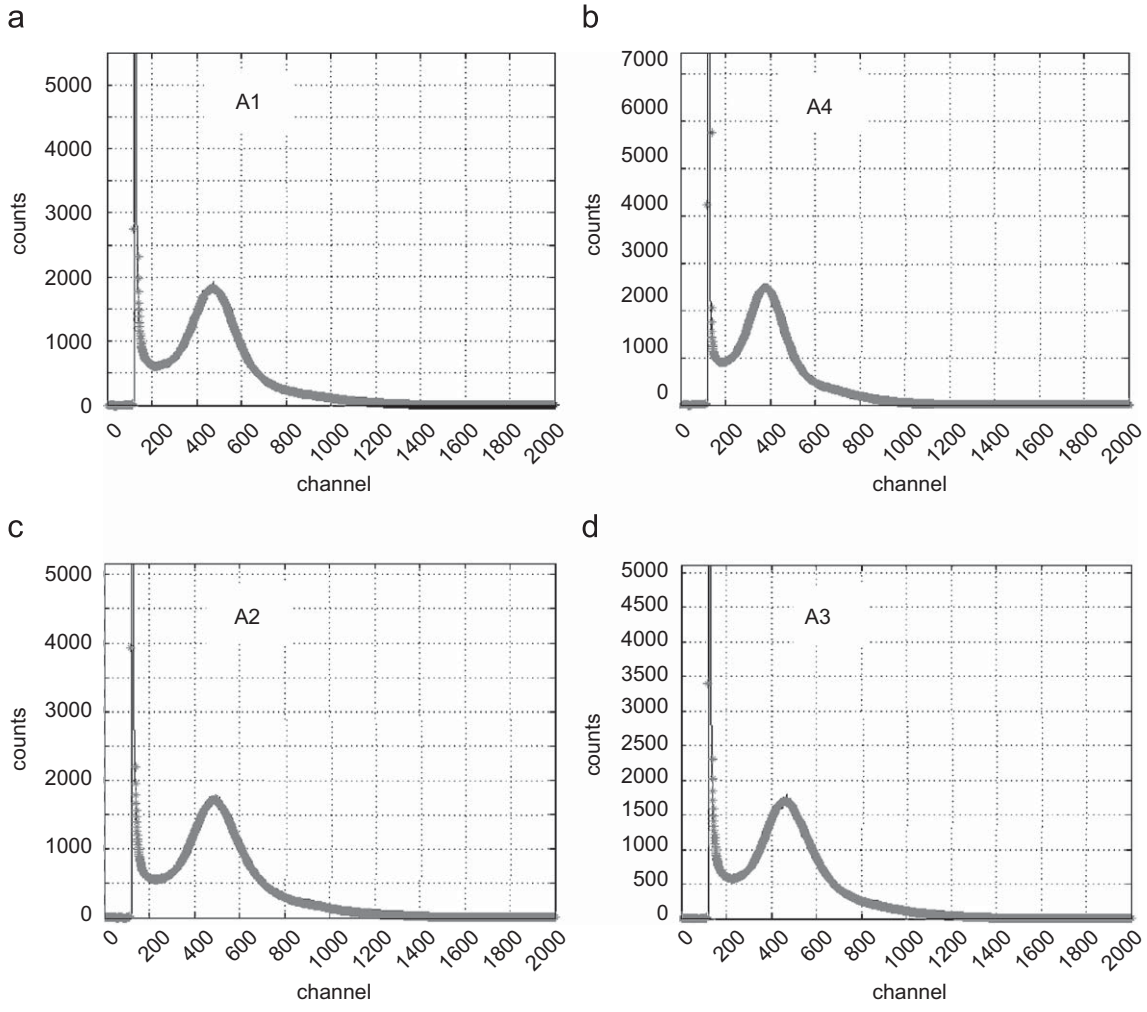

Fig. 7. The single photon spectrum for each anode in the ZF0025 sample. Each channel corresponds to 0.170 pC.

Please cite this article as: S. Aiello, et al., Nucl. Instr. and Meth. A (2009), doi:10.1016/j.nima.2009.03.235

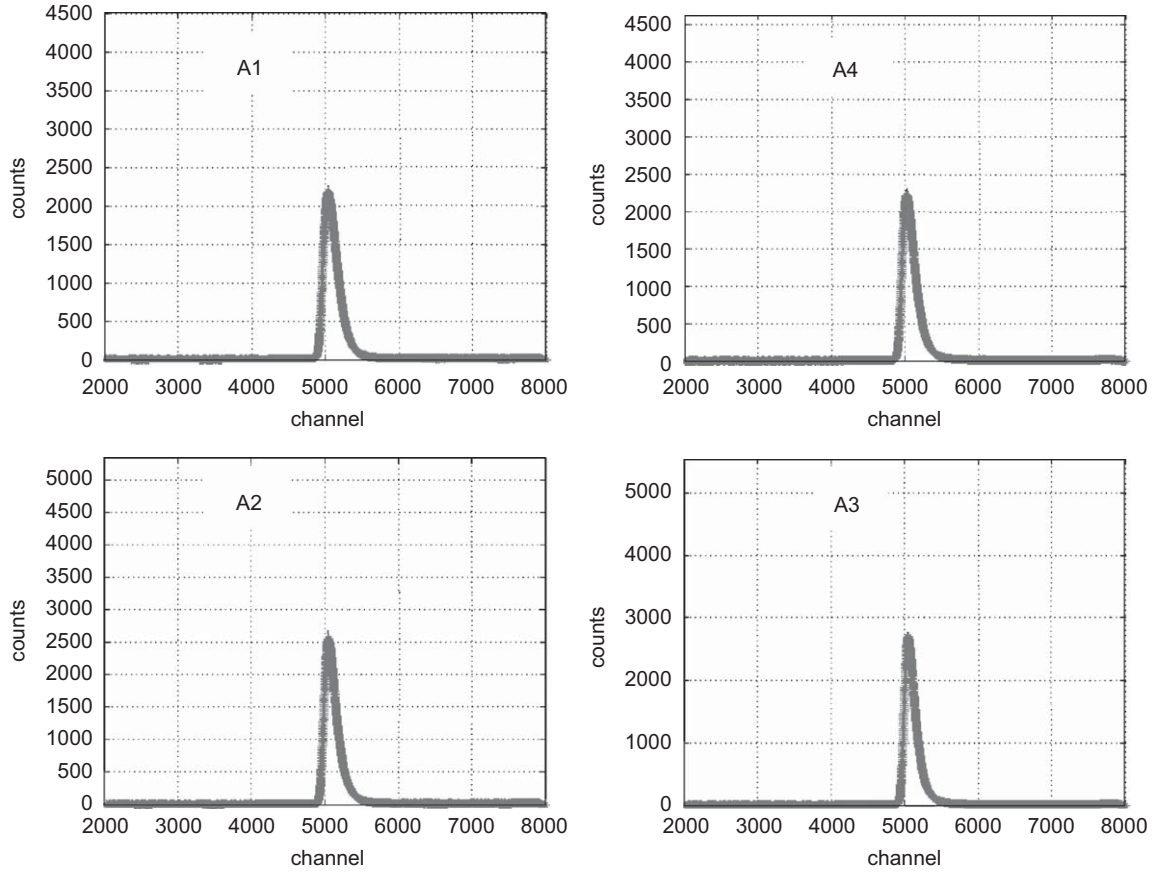

Fig. 8. The timing distribution of the single photon for each anode in the ZF0025 sample. Each channel corresponds to 25 ps.

Table 3
Summary of the ZF0025 photomultiplier properties at a HV of 1550 V.

Anode	A1	A2	A3	A4
P/V	3.03	3.09	2.95	2.75
Gain [$\times 10^7$]	5.0	5.4	5.0	3.9
RSE (%) (sigma)	33.6	30.6	37.3	35.2
TT (ns)	105	106	106	105
TTS (ns) (FWHM)	4.6	4.0	3.5	4.2

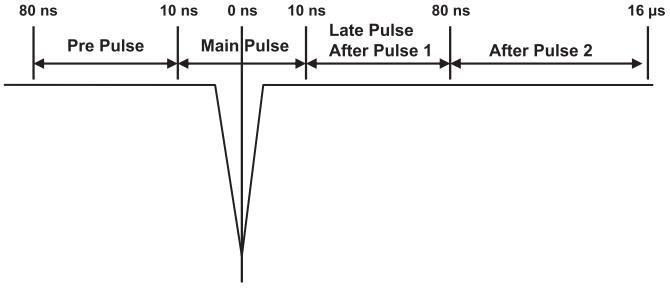

Fig. 9. The adopted definition of pre- and after pulses.

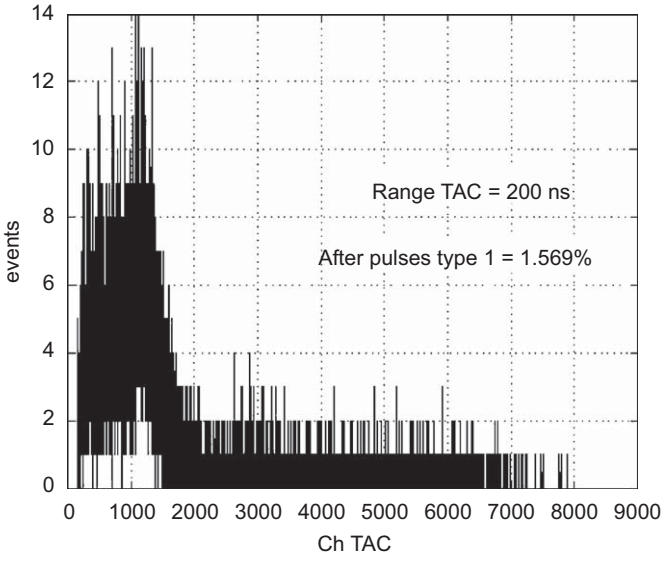

Fig. 10. The time distribution of the Type 1 After pulse for anode A1 in the ZF0025 sample.

- Late pulse: pulses arriving at 10–80 ns after the main pulse, when the main pulse is not present.
- After pulse 1: spurious pulses arriving at 10–80 ns after the main pulse.
- After pulse 2: spurious pulses arriving at 80 ns–16 μs after the main pulse.

Late pulses and After pulses 1 differ in that the former are believed to arise from photoelectron backscattering on the first

Please cite this article as: S. Aiello, et al., Nucl. Instr. and Meth. A (2009), doi:10.1016/j.nima.2009.03.235

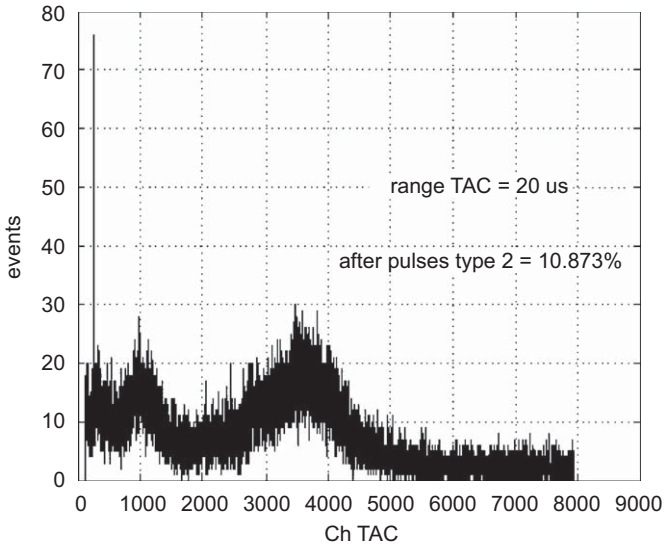

Fig. 11. The time distribution of the Type 2 After pulse for anode A1 in the ZF0025 sample.

Table 4
Summary of spurious pulses for sample ZF0025.

Anode	A1	A2	A3	A4
Pre-pulses (%)	0.05	0.18	0.24	0.05
Late pulses (%)	7.74	7.96	7.14	6.50
After pulses 1 (%)	1.57	1.91	1.68	1.22
After pulses 2 (%)	10.87	12.53	13.49	10.41

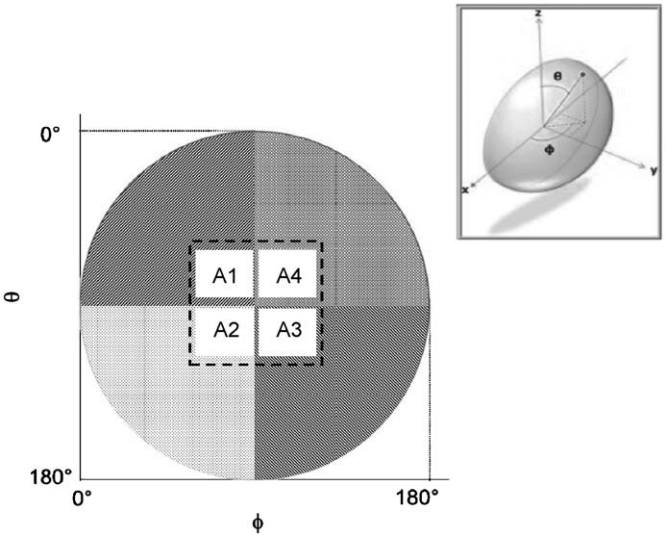

Fig. 12. The reference system adopted in the measurements. In the top-right the hemispherical surface of the photocathode is shown: the photomultiplier is aligned along the y-axis and the top of the photocathode corresponds to $\theta = 90^{\circ}$ and $\phi = 90^{\circ}$. The circle represents the shape of the photomultiplier as seen from a point along the y-axis. The correspondence between the angles and the four anodes is also shown.

dynodes, and the latter are believed to originate from the ionization of the residual gas atoms and the atoms adsorbed by the first dynode surface.

A typical distribution of After pulses 1 and 2 is reported in Figs. 10 and 11, respectively. A summary of the spurious pulses is given in Table 4. The values represent the ratio of the number of spurious pulses to the number of main pulses, expressed as percentages.

3.3. The local response

To be used in a direction-sensitive optical module the multianodic photomultiplier should be able to identify precisely the position of the photocathode emission point. Therefore the response of the photomultiplier was studied for each anode individually, by illuminating the photocathode area with a single-photon pulsed beam with 5 mm-diameter. A scan of the photocathode surface was performed using a 324-points grid.

The angle definition adopted to represent the results is shown in Fig. 12. In Fig. 13 the area of the single photon peak is reported for each anode. The area includes all the events with a charge corresponding to more than 1/3 photoelectrons. The largest measured values are represented in red and the smallest, equal to less than 2% of the largest measured value, in blue. Comparing the response of the four anodes it is evident that each anode is sensitive to approximately one-fourth of the photocathode area with small differences in the shape of the transition region between the various quarters.

In Fig. 13 it can also be observed that each anode shows a residual sensitivity (in the order of few %) to the remaining photocathode area. This could affect the performance of the direction-sensitive optical module. Therefore we investigated the origin of the effect in more detail using the oscilloscope to monitor the shape of the four anode signals when the centre of the photocathode sector connected to anode A1 is illuminated. In Fig. 14 the shape of the signals is reported. The effect is shown for a laser intensity corresponding to an average of 15 photoelectrons, but it is the same for the whole dynamic range studied. The figure shows that, in coincidence with the regular unipolar signal, the coupling between the dynodic chains generates three oscillating parasitic outputs. The parasitic signals have amplitudes of approximately 16% of the regular signal and a charge $\approx$ 3% of the good one. Therefore the residual sensitivity that appears in Fig. 13 is largely related to those parasitic signals that exceed the thresholds of the acquisition system. We expect to reduce the cross-talk by analysing the different shapes of the parasitic signals and work is currently in progress on the design of an electronic board dedicated to this task.

It is worth noting that if the measurements reported in Fig. 13 are compared with the typical surface of the standard photocathode as reported in Fig. 15 the result is that the effective photocathode area extends up to the geometrical limit of the photomultiplier hemisphere, while the standard 10-in. photomultiplier shows a reduced surface. From purely geometrical considerations we have estimated that the prototype could collect up to 20% more light.

We are presently developing an optical module equipped with the 4-anodic prototype in order to measure how the directionality and the larger sensitive area could improve the performance of this device. The results will be reported and discussed in a further paper.

4. Conclusions

We tested two prototypes of a large area (10-in.) hemispherical multianodic photomultiplier manufactured by Hamamatsu. The measurements show good linearity up to 100 photoelectrons, a gain higher than 10^7 and a gain uniformity better than 10% with

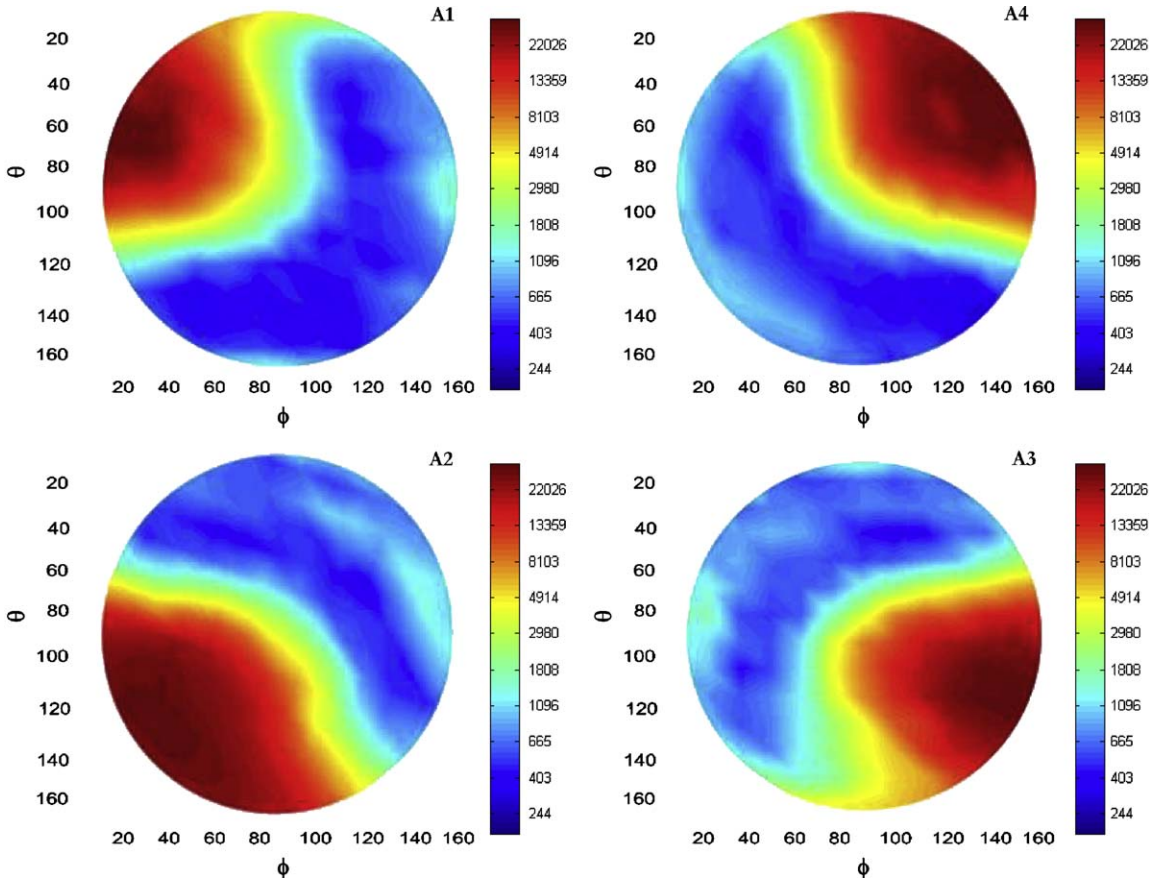

Fig. 13. The local response of the photocathode to a single photoelectron for each anode of the ZF0025 prototype.

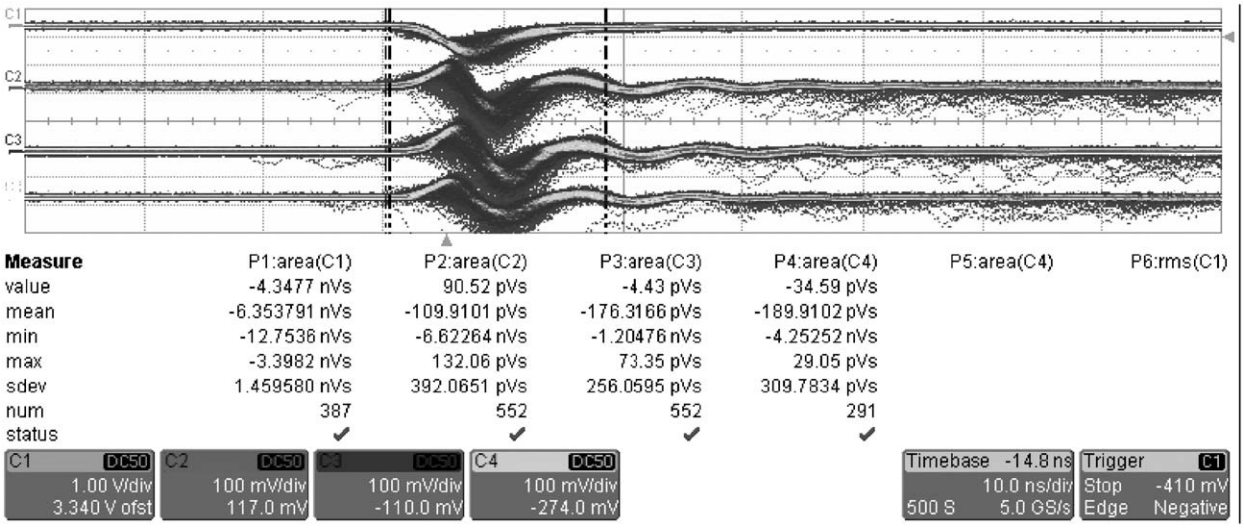

Fig. 14. The effect of the coupling between the four ZF0025 dynodic chains. C1 represents the active anode. C2, C3 and C4 are plotted in a $\times 10$ expanded scale to enhance the effect. Each division on the *x* axis corresponds to 10 ns.

only one anode that differs by $\approx 25\%$ due to the quality of the dynodes. The prototype performances are fully in line with the KM3NeT specification. By scanning the photocathode surface with a thin light beam we verified that there is less than 3% cross-talk between the prototype anodes. The cross-talk is mainly generated by the capacitive coupling of the four dynodic chains and could be further reduced with a pulse shape analysis using a dedicated electronics. Finally the shape of the first dynode allows the photocathode surface to be enlarged providing 20% more collected light compared to a standard Hamamatsu 10-in. photomultiplier.

Please cite this article as: S. Aiello, et al., Nucl. Instr. and Meth. A (2009), doi:10.1016/j.nima.2009.03.235

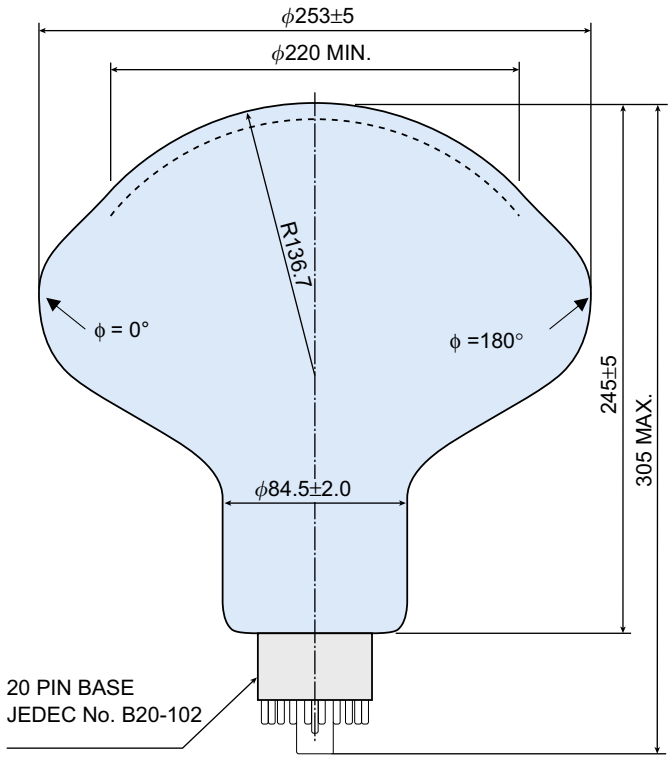

Fig. 15. The section of the Hamamatsu photomultiplier at $\theta = 90^\circ$. The dashed line represents the typical coverage of the photocathode for the standard 10-in. The points corresponding to $\phi = 0^\circ$ and 180° are also shown. The drawing has been taken from Hamamatsu data sheets [22]. The meaning of θ and ϕ is given in Fig. 12.

Acknowledgements

The authors wish to thank Hamamatsu Photonics for their help in producing the prototypes of the multianodic large area photomultiplier. This work was supported in part by the Italian Istituto Nazionale di Fisica Nucleare and the KM3NeT Design Study, funded by the EU through FP6, Contract no. 11937.

References

[1] P. Amram, et al., ANTARES Collaboration, Nucl. Instr. and Meth. A 484 (2002) 369 [arXiv:astro-ph/0112172].
[2] K. Hanson, O. Tarasova, IceCube Collaboration, Nucl. Instr. and Meth. A 567 (2006) 214.
[3] R.I. Bagduev, et al., Nucl. Instr. and Meth. A 420 (1999) 138 [arXiv:astro-ph/9903347].
[4] E.G. Anassontzis, et al., NESTOR Collaboration, Nucl. Instr. and Meth. A 479 (2002) 439.
[5] ⟨http://www.km3net.org/CDR/CDR-KM3NeT.pdf⟩.
[6] ⟨http://www.km3net.org⟩.
[7] A. Braem, C. Joram, J. Seguinot, P. Lavoute, C. Moussant, Nucl. Instr. and Meth. A 570 (2007) 467.
[8] P.C. Bosetti, An Optical Sensor for DUMAND II, Proc. 23rd ICRC (Calgary), vol. 4, 1993, p. 534.
[9] B.K. Lubsandorzhev, BAIKAL and TUNKA Collaboration, Nucl. Instr. and Meth. A 442 (2000) 368.
[10] P. Kooijman, Nucl. Instr. and Meth. A 567 (2006) 508.
[11] B.K. Lubsandorzhiev, R.V. Vasiliev, Y.E. Vyatchin, B.A.J. Shaibonov, Nucl. Instr. and Meth. A 567 (2006) 12 [arXiv:physics/0601157].
[12] E. Migneco, et al., Nucl. Instr. and Meth. A 567 (2006) 444.
[13] M. Anghinolfi, et al. INFN Note INFN-TC-08-2, available at ⟨http://www.lnf.infn.it/sis/preprint/⟩, 2008.
[14] M. Taiuti, Nucl. Instr. and Meth. A 525 (2004) 137.
[15] M. Brunoldi, et al., INFN Note INFN-TC-07-9, available at ⟨http://www.lnf.infn.it/sis/preprint/⟩, 2007.
[16] ⟨http://www.picoquant.com/⟩.
[17] ⟨http://www.ophiropt.com/⟩.
[18] A. Savasta, Thesis, Universitiy of Catania (in Italian), 2007.
[19] E. Leonora, Nucl. Instr. and Meth. A 602 (2009) 217.
[20] Private communication.
[21] J.A. Aguilar, et al., ANTARES Collaboration, Nucl. Instr. and Meth. A 555 (2005) 132 [arXiv:physics/0510031].
[22] Photomultiplier tubes and assembly for scintillation counting & high energy physics, Hamamatsu catalog.
[23] KM3NeT conceptual design report for a deep-sea research infrastructure incorporating a very large volume neutrino telescope in the mediterranean sea ⟨http://www.km3net.org/design.php⟩.

Please cite this article as: S. Aiello, et al., Nucl. Instr. and Meth. A (2009), doi:10.1016/j.nima.2009.03.235